Planetary and Space Science 77 (2013) 126–135

Contents lists available at SciVerse ScienceDirect

Planetary and Space Science

journal homepage: www.elsevier.com/locate/pss

Modeling the seasonal variability of the plasma environment in Saturn's magnetosphere between main rings and Mimas

W.-L. Tseng *, R.E. Johnson, M.K. Elrod

University of Virginia, Charlottesville, VA 22904, USA

ARTICLE INFO

Article history:
Received 22 December 2011
Accepted 3 May 2012
Available online 11 May 2012

Keywords:
Saturn's rings
Plasma composition
Magnetosphere
Seasonal variability

ABSTRACT

The detection of O_2^+ and O^+ ions over Saturn's main rings by the Cassini INMS and CAPS instruments at Saturn orbit insertion (SOI) in 2004 confirmed the existence of the ring atmosphere and ionosphere. The source mechanism was suggested to be primarily photolytic decomposition of water ice producing neutral O_2 and H_2 (Johnson et al., 2006). Therefore, we predicted that there would be seasonal variations in the ring atmosphere and ionosphere due to the orientation of the ring plane to the sun (Tseng et al., 2010). The atoms and molecules scattered out of the ring atmosphere by ion–molecule collisions are an important source for the inner magnetosphere (Johnson et al., 2006; Martens et al., 2008; Tseng et al., 2010, 2011). This source competes with water products from the Enceladus' plumes, which, although possibly variable, do not appear to have a seasonal variability (Smith et al., 2010). Recently, we found that the plasma density, composition and temperature in the region from 2.5 to 3.5 R_S exhibited significant seasonal variation between 2004 and 2010 (Elrod et al., submitted for publication). Here we present a one-box ion chemistry model to explain the complex and highly variable plasma environment observed by the CAPS instrument on Cassini. We combine the water products from Enceladus with the molecules scattered from a corrected ring atmosphere, in order to describe the temporal changes in ion densities, composition and temperature detected by CAPS. We found that the observed temporal variations are primarily seasonal, due to the predicted seasonal variation in the ring atmosphere, and are consistent with a compressed magnetosphere at SOI.

Published by Elsevier Ltd.

1. Introduction

Saturn's oxygen ring atmosphere and ionosphere was discovered by the Cassini spacecraft in 2004. Both the Ion and Neutral Mass Spectrometer (INMS) and the Cassini Plasma Analyzer (CAPS) detected O_2^+ and O^+ ions over the main rings during the Saturn Orbital Insertion (SOI) in 2004 (Tokar et al., 2005; Waite et al., 2005) as well as a comparable component of electrons (Coates et al., 2005). Johnson et al. (2006) suggested that the primary source is photolytic decomposition of water ice producing neutral O_2 and H_2. The measurements also indicated that the ion–molecule collisions between the newly formed ions O_2^+/O^+ and neutral O_2 determined the ion density distribution detected by CAPS at high altitudes above the main rings. Using the photolytic model we also predicted that there would be significant seasonal variations in the density of the ring atmosphere and ionosphere since the neutral O_2 production rate depends on the solar incident angle with respect to the ring plane (Tseng et al., 2010). The ion–molecule collisions, which account for the observed vertical distribution, also scatter O_2, H_2, O and H beyond the ring plane into the magnetosphere and into Saturn's atmosphere. Once ionized, they are a source of O_2^+ and H_2^+ ions in the magnetosphere seen by Cassini Magnetospheric Imaging Instrument (MIMI) (Krimigis et al., 2005) and CAPS (Martens et al., 2008; Tseng et al., 2011). Therefore, the seasonal variations should also be reflected in the density of these ions in the region outside the main rings.

However, the suggested seasonal variations are complicated by the deposition of water products from the Enceladus' plumes onto the A-ring as described by measurements and modeling (Jurac and Richardson, 2007; Farrell et al., 2008; Cassidy and Johnson, 2010). As with the dissociated oxygen in the ring atmosphere, the absorbed oxygen rich ions and neutrals from the Enceladus torus could be recycled via grain-surface chemistry contributing to the atmosphere over the main rings and the atoms and molecules scattered into the magnetosphere (Tseng and Ip, 2011). Hansen et al. (2011) monitored the Enceladus plume activity using the Cassini Ultraviolet Imaging Spectrograph (UVIS) and found that they appeared to be stable. Although the INMS measurements suggested the source rate is variable (Smith et al., 2010), no seasonal variability was apparent. So, the Enceladus torus contribution to the ring atmosphere can mitigate the

* Corresponding author.
E-mail address: wt7b@virginia.edu (W.-L. Tseng).

0032-0633/$ - see front matter Published by Elsevier Ltd.
http://dx.doi.org/10.1016/j.pss.2012.05.001

seasonal variation in the ring atmosphere. Despite the uncertainties in the recycling efficiency, the non-detection (or upper limit) of H_2^+ ions over the B-ring by the Cassini CAPS at SOI has helped constrain the source rates (Tseng et al., 2011).

Elrod et al. (submitted for publication) examined the CAPS plasma data between 2.5 and 3.5 R_S from 2004 to 2010 including a comparison with Voyager 2 data from Richardson (1986) where R_S is one mean Saturn radius (60,300 km). They showed that there were large variations over that time period in the ion density, temperature and composition. A significant drop in the ion density and temperature was found between 2005 and 2010 as compared to Voyager 2 data and Cassini data at SOI (2004). They also found that the O_2^+ was the dominant heavy ion at SOI, but the O_2^+ density was comparable to or less than the water-group ion (hereafter referred to as W^+) density in the period of 2005–2010. Using preliminary results from the model described in detail here, they concluded that, although the possible variability in the Enceladus source might contribute, the observed variations were primarily seasonal due to the predicted seasonal variation in the ring atmosphere.

In this work, we developed a one-box ion chemistry model for the plasma in the region between 2.5 and 3.5 R_S to explain the complex and highly variable plasma environment that was detected by CAPS. First, an updated ring atmosphere model is described in Section 2, since this atmosphere is affected by the recently observed change in the ring particle temperatures from solstice to equinox which was absent in our earlier model (Tseng et al., 2010). In Section 3, our ion-chemistry model, combining the Enceladus torus and the seasonal ring atmosphere sources, is presented. The simulations are carried out for both SOI and equinox conditions and the results are in a remarkable agreement with the trends found in the CAPS data. In Section 4, we solved a set of continuity equations for the plasma energy in order to understand the low ion temperature detected after SOI. It is found that ion energy lost to momentum transfer during ion–molecule collisions can roughly account for decrease of ion temperature. Finally, a summary is given in Section 5.

2. Revised ring atmosphere model: neutral source rates of O_2 and H_2 at SOI and equinox

In our previous paper (Tseng et al., 2010), we studied the structure and time variability of Saturn's ring atmosphere and ionosphere using a fixed ring temperature $T=100$ K accounting only for the change in solar UV flux on the O_2 production rate. However, the average temperature of Saturn's ring particles also changes significantly with the change in the solar incident angle as revealed by the Cassini Composite Infrared Spectrometer (CIRS) data (Flandes et al., 2010): $T\sim100$ K at solstice and $T\sim60$ K at equinox. Since this change primarily occurs for the A- and B-ring particles, which are the principal source of the ring atmosphere, the photo-production of O_2 and H_2 and recycling on the ring particles are significantly modified by this change in the particle temperatures. Therefore, we re-examine the time variability of Saturn's ring atmosphere and ionosphere allowing for the effect of solar illumination angle and the ring particle temperature. In addition we consider the influence of the deposition of oxygen from Enceladus torus onto the A-ring.

O_2 production by UV photons depends on the UV flux and, hence, on the solar incident angle with respect to the ring plane as well as the ring particle temperature. In our earlier work in 2010, we used $Q(O_2)=c\times10^6$ molecules cm^{-2} s^{-1} with a fixed ring temperature $T=100$ K. This was based on the model in Johnson et al. (2006) to describe the observed plasma densities primarily over the B-ring with the parameter c accounting for recycling of dissociated oxygen and oxygen ions on the ring particle surfaces. At $T=100$ K and solar incident angle $\gamma=24^\circ$ the neutral O_2 source rate was computed from laboratory data to be $\sim1.0\times10^{26}$ s^{-1} at SOI due to photolytic decomposition of water ice. Since the calculated ion densities were roughly a factor of 20 smaller than our recent re-analysis of the CAPS data over the B-ring at SOI (Elrod et al., submitted for publication), the effective source at SOI was estimated to be $\sim2.0\times10^{27}$ s^{-1} ($c\sim20$) accounting for recycling (e.g. Johnson et al., 2006), the influences of Enceladus' plumes (Tseng and Ip, 2011), the solar activity and, possibly, the simplified ion–molecule interactions.

Earlier we estimated a photolytic O_2 source rate $\sim1.0\times10^{25}$ s^{-1} near equinox again assuming an average ring particle temperature of $T=100$ K (Tseng et al., 2010). Using the same model but with an average temperature of ~60 K near equinox (Flandes et al., 2010), the photolytic source rate is severely quenched by a factor of $\exp(-\alpha/kT)$ where α is an activation barrier, which is somewhat uncertain. Here we use $\alpha\sim0.03$ eV for the photo-production of O_2 (e.g., Johnson, 2011). Using $T=60$ K as the average temperature of the particles gives a photolytic yield a factor of ~10 reduction, in addition to the decrease due to the solar illumination angle, or $\sim1.0\times10^{24}$ s^{-1}. In absence of CAPS data over the main rings near equinox, we allow that recycling of desorbed oxygen and the contribution of oxygen from Enceladus could also enhance this source rate by the same factor as summarized in Table 1. Fortunately, the conclusions discussed below are not critically dependent on the exact size of the equinox ring atmosphere source rate, but only on the fact that the source rate is significantly smaller than that at SOI.

The momentum transfer during collisions between primarily O_2^+ ions and neutral O_2 molecules creates a component of O_2 molecules scattered into the magnetosphere (Johnson et al., 2006; Martens et al., 2008; Tseng et al., 2010). Fig. 1 shows the calculated radial profiles of the neutral O_2 column density from the rings to a radial distance of 10 R_S for the SOI and equinox source rates and for an intermediate source rate. Once ionized, they contribute to the local magnetospheric plasma. It is seen that the neutral O_2 column density over the main rings can be roughly scaled to the O_2 source rate. But, outside the main rings, the scattered population formed by ion–molecule collisions changes nearly quadratically with the source rate, as it depends on both the neutral and the ion density. That is, when the O_2 source rate becomes ten percent of SOI source rate, the scattered O_2 column density outside the main rings drops to be roughly one percent of SOI value.

The azimuthally symmetric spatial distributions of the O_2^+ ions produced by photoionization over the main rings are shown in Fig. 2 for (a) equinox and (b) SOI phase. It is clearly seen that the O_2^+ source rate depends on the orientation of the ring plane to the Sun with the O_2^+ density significantly lower at equinox. The structure and main features (such as the asymmetry above and

Table 1
Summary of the neutral O_2 and H_2 source rate of main rings.

Source rate (s^{-1})	SOI ($Y=24^\circ$ & $T=100$K)	Equniox ($Y=2^\circ$ & $T=60$K)
O_2[a]	1.0×10^{26}	1.0×10^{24}
O_2[b]	2.0×10^{27}[c]	2.0×10^{25}
H_2[a]	2.0×10^{26}[d]	2.0×10^{24}

[a] Photolytic source rate.
[b] Corrected for recycling which includes contributions of oxygen from Enceladus deposited on the A-ring (see discussion in Section 2).
[c] Correction based on calibration to the CAPS SOI data (Elrod et al., submitted for publication).
[d] No detection (or upper-limit) of H_2^+ to help us constrain the neutral H_2 source.

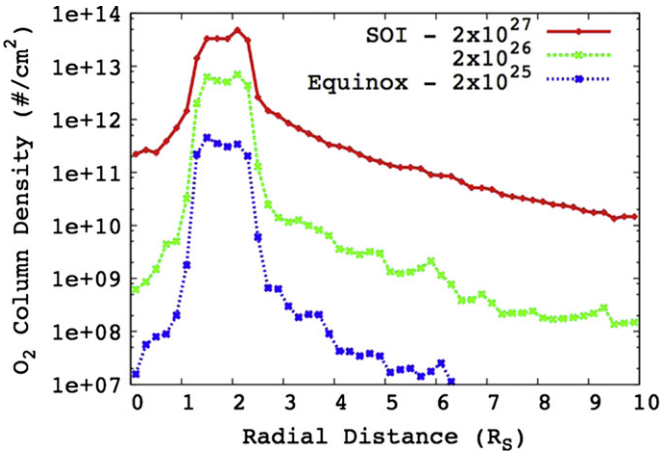

Fig. 1. Radial distributions of the neutral O_2 column density with a source rate $\sim 2\times 10^{27}$ O_2 s^{-1} (SOI phase), $\sim 2\times 10^{26}$ O_2 s^{-1} (intermediate phase) and $\sim 2\times 10^{25}$ O_2 s^{-1} (equinox phase), respectively.

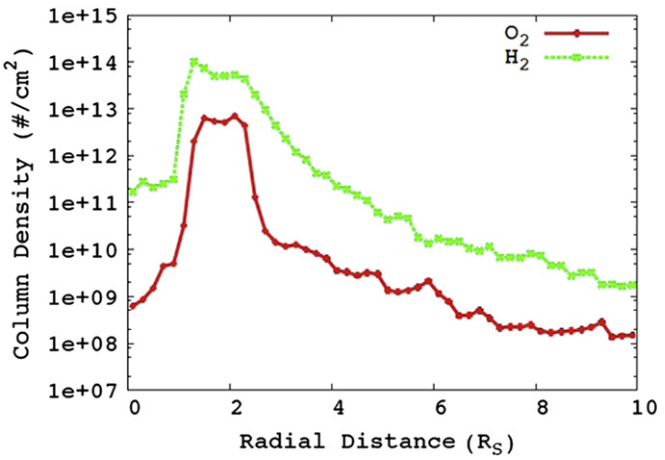

Fig. 3. Radial distributions of the neutral O_2 and H_2 column density with a source rate of $\sim 2\times 10^{26}$ H_2 s^{-1} and of $\sim 1\times 10^{26}$ O_2 s^{-1}, respectively, which ignores the enhancements in Table 1.

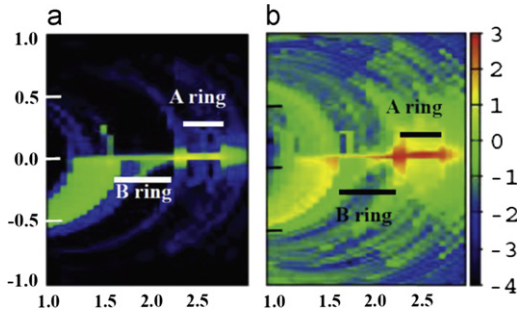

Fig. 2. O_2^+ ion density in Log 10 scale as indicated in a color bar. *X*-axis is the radial distance (R_S). *Z*-axis is the vertical distance (R_S). (a) Equinox phase: photolytic source rate: 2.0×10^{25} s^{-1}, (b) SOI phase: source rate: 2.0×10^{27} s^{-1}. (For interpretation of the references to color in this figure legend, the reader is referred to the web version of this article.)

below the ring plane) of the ring ionosphere have been explored in Johnson et al. (2006) and Tseng et al. (2010). Although the calculated ion densities involve considerable uncertainties such as the recycling of oxygen on grain surfaces, we note that, if the ring source rate is not overwhelmed by material from Enceladus, the seasonal excursion in the size of Saturn's O_2 ring atmosphere and ionosphere combining the effects of solar incident angle and ring temperature might be much larger than predicted earlier (Tseng et al., 2010), with the densities at solstice around two orders of magnitudes higher than near equinox.

Both neutral O_2 and H_2 molecules are released in a ratio of 1:2 from the main rings by decomposition of ice by solar UV photons (Johnson et al., 2006). We carried out the simulations of the spatial morphology of the ring H_2 atmosphere and the ring H_2^+ ionosphere including the ion–molecule collisions between H_2 (H_2^+) and O_2^+/W^+ (O_2/W) (Tseng et al., 2011). Fig. 3 shows the radial distributions of the neutral O_2 and H_2 column density with a source rate of $\sim 2\times 10^{26}$ H_2 s^{-1} and of $\sim 1\times 10^{26}$ O_2 s^{-1}, respectively. Overall, the neutral H_2 column density over the main rings is approximately one order of magnitude larger than O_2 since H_2 has a longer photolytic lifetime. Compared to O_2, H_2 attains a larger thermal velocity on thermal desorption from the ring particles and obtains more energy during ion–molecule collisions because of its smaller mass. Therefore, in the region between the main rings and Enceladus, our model of the column density of scattered H_2 is roughly two orders of magnitudes higher than our model O_2 column density but the number density of H_2 near the equatorial plane is only roughly one order of magnitude higher. In addition, Tseng et al. (2011) found that, during periods where the ring source rate of 2×10^{26} H_2 s^{-1} applies, H_2 scattered from the ring atmosphere and photodissociation of water from Enceladus are comparable sources in the magnetosphere between ~ 6 and ~ 2.5 R_S. At any time, Titan is the dominant source of H_2 in the outer magnetosphere. The density distribution of H_2^+ outside the main rings estimated from our model (Tseng et al., 2011) roughly agrees with the CAPS observations (Thomsen et al., 2010). In addition, we note that, CAPS should have detected H_2^+ in Cassini division if H_2 and O_2 are formed stoichiometrically (Tseng et al., 2011). Since CAPS did not detect H_2^+ over the main rings at SOI (Young et al., 2005; Tokar et al., 2005), it is likely that the same enhancement factor used for O_2 recycling does not apply since the H produced by dissociation has a higher velocity and is lost from the region (Johnson et al., 2006). Either non-detection (an upper limit) over the rings or measurement of H_2^+ in the magnetosphere can be used to constrain the H_2/O_2 source mechanism from main rings.

3. Ion chemistry model

As mentioned before, in Elrod et al. (submitted for publication) we have shown that there were significant temporal variations in the plasma density and composition in the region 2.5–3.5 R_S over the period 2004–2010. We also discussed the possible explanations such as the seasonal variability in the ring atmosphere, variability in the Enceladus source rate, and variability in solar activity. To further understand the CAPS observations and examine the roles of Enceladus and of the ring atmosphere source we developed a one-box ion chemistry model to simulate the complex and highly variable plasma environment that was observed by the Cassini CAPS. Some preliminary results for the model described here were reported in Elrod et al. (submitted for publication). The plasma chemistry between 2.5 and 3.5 R_S near Saturn's equatorial plane is described by the following parameters: the neutral densities, the diffusion loss timescale, and the density and temperature of hot electrons. The ionization, recombination, ion–molecule reactions and charge exchange for the major neutral species (neutral H_2O, OH, O, H, H_2 and O_2) are also included. The output is the steady-state plasma composition (H_3O^+, H_2O^+, OH^+, O^+, H^+, H_2^+, O_2^+ as well as the thermal electron density). The thermal electron density is a sum of the ion densities. The photo-ionization rates are from Huebner et al. (1992). The cross-sections for electron impact ionization are based

on Itikawa and Mason (2005), Itakawa (2009), Kim and Desclaux (2002), Yoon et al. (2008) and Shah et al. (1987). Maxwellian energy distributions are assumed in calculating the electron–ion and electron–neutral reaction rates. In this region, the suprathermal electron density is nearly depleted (Schippers et al., 2008). But there is a small population of the intermediate hot electrons of T_e=20–30 eV and 40–50 eV which are mainly from photoionization of water-group neutrals (Schippers et al., 2009). This hot-electron population is set to be 0.1 cm^{-3} (Schippers et al., 2009). The thermal electrons, initially assumed to have T_e=2.0 eV (e.g. Gustafsson and Wahlund, 2010) were shown to primarily affect the electron–ion recombination rates, which are derived from Schreier et al. (1993). Ion–molecule reaction rates are calculated with energy-dependent cross-sections when available with the relative speed determined by both the plasma corotation velocities and the keplerian velocities of neutrals at 3.0 R_S. Energy independent reaction rates are used when the data is insufficient. Here, applying a Maxwellian energy distribution for the ions in the ion–molecule reactions is not so important since most of reaction rates are energy independent (as seen in Appendix 1). We also find that using a Maxwellian energy distribution results in only ~20% difference for the energy-dependent cross-sections involving collisions between water-group neutrals and ions.

The rates (listed in Appendix 1) are used in a set of continuity/chemical rate equations for each ion species, $dn_i/dt=S_i-L_i$ with the source rate, S_i, and the loss rate, L_i. Using the neutral density distributions from the ring atmosphere and the Enceladus torus, the initial values of densities of each ion species were assigned to be zero and the densities at steady state were solved for using various test parameters. The ion sources (S_i) are photoionization, electron-impact ionizations and ion–molecule reactions with the neutrals. The loss (L_i) to ion–molecule reactions and recombination are also included and the radial diffusion is treated as a constant loss rate. The coupled set of equations is solved iteratively using the 4th order Runge–Kutta method to reach the steady-state.

3.1. Modeling at SOI

For the electron properties described above, photoionization is the primary ion source in this region with the hot-electron impact ionization accounting for ~30%. loss by radial diffusion (~2 months; Rymer et al., 2008) was found to be dominated by recombination in agreement with the statement in Sittler et al. (2008): 'recombination loss for molecular ions dominated in inner magnetosphere inside Dione while diffusion loss dominated in outer magnetosphere'. In our model, recombination is the primary loss process for H_3O^+ and O_2^+, whereas ion–molecule reactions and recombination compete for the loss of H_2O^+ and OH^+. Atomic ions, like O^+ and H^+, are neutralized directly in ion–molecule collisions or indirectly by ion–molecule reactions in which a molecular ion is formed and subsequently lost by recombination.

To understand the situation at SOI, we consider a neutral background of O, OH and H_2O supplied by the Enceladus torus with an average source rate of 1×10^{28} H_2O s^{-1} from Cassidy and Johnson (2010) and the O_2 and H_2 clouds scattered from the ring atmosphere as discussed in Section 2. Since there was no detection of H_2^+, we assumed an arbitrary enhancement factor of 5 for the neutral H_2 ring source rate due to recycling. This is a reasonable assumption, since at an enhancement factor as high as 20 suggested for O_2, CAPS would have detected H_2^+ at SOI (Tseng et al., 2011). Whereas the Enceladus torus dominates the total neutral column densities in this region (Elrod et al., submitted for publication), the significant difference in scale heights (ring atmosphere ~1000 km for O_2 and ~4000 km for H_2; Enceladus torus water products ~6500 km) are such that the near equatorial density is dominated by the ring atmosphere at SOI. The average neutral densities near the equator around 3.0 R_S are shown in Table 2. At SOI, the averaged photoionization rates (Huebner et al., 1992) are applied since the solar activity was average. Using these densities, we find that O_2^+ is the dominant ion in this region with a density ~150 cm^{-3} about the same order of magnitude as the average CAPS data ~500 cm^{-3} (Elrod et al., submitted for publication). The total water-group ion density calculated is ~20 cm^{-3} as compared to the CAPS data (~150 cm^{-3}). H_3O^+ is the major water-group ion in our model because of the efficient ion–molecule reactions at the relative speeds considered here. H_3O^+ is primarily formed by the reaction of H_2O^+ with H_2 where the H_2 component from the ring source is significant at SOI. Although both densities are lower than the average CAPS data in this region, the ratio of O_2^+/W^+ (~7.5) is higher than the ratio found in CAPS SOI data (~2.5–4.5). Therefore, our basic model using average conditions requires modification as discussed below and in Section 3.3. The O_2^+ and W^+ ion densities and the ratio of O_2^+/W^+ from the CAPS SOI data between 2.4 and 2.8 R_S (see Figure 5 and 6 in Elrod et al., submitted for publication) also appear to increase toward Enceladus. These increases are likely due to spacecraft trajectory as Cassini was passing through the ring plane from the northern side to the southern side.

Table 2
Neutral background for SOI case.

Species	Equatorial density (cm^{-3})	Source (Ref.)
H_2O	2000	Enceladus torus with an average source rate of 1×10^{28} H_2O s^{-1} (Cassidy and Johnson, 2010)
OH	1000	Enceladus torus (Cassidy and Johnson, 2010)
O	1000	Enceladus torus (Cassidy and Johnson, 2010)
H_2	1000	Photodissociation of Enceladus water torus (Tseng et al., 2011)
O_2	20,000	Ring atmosphere with an O_2 source rate of 2×10^{27} s^{-1} referred to CAPS data at SOI
H_2	250,000	Ring atmosphere with a H_2 source rate 1×10^{27} s^{-1} with an enhancement factor of 5 due to recycling (Tseng et al., 2011)
Immediate-hot electron	0.1	Photoelectron from ionization of water-group neutrals (Schippers et al., 2009)

Overall, the total ion densities at SOI in the above model are about 4 times lower than the CAPS data. This also suggests that the plasma environment at SOI differs from the average conditions described above. The effect of solar activity on the neutral density and, hence, on ion formation are mostly included in our scaling of the source rate. However, we do note that the total ion density obtained from Voyager 2 data near equinox in 1981 at solar maximum was intermediate to the CAPS data at SOI, which occurred at solar average, and the CAPS data near equinox, which occurred at solar minimum (Elrod et al., submitted for publication). This suggests that solar activity might play an important role. Related to this, we note that Saturn's magnetosphere was very compressed at SOI as a result of an 'active solar wind' and the total electron energy at SOI was ~25% higher than the average used above (Rymer, private communication). Hot plasma injection was also identified during SOI, which is indicative of tail reconnection due to significant compression and is related to the corotating interaction (CIR) region (Bunce et al., 2005). Although the data averaged over a number of orbits shown in Schippers et al. (2008) suggested that the suprathermal electron is nearly depleted in the inner magnetosphere, the hot electron temperature and fraction can vary significantly in inner

magnetosphere (e.g. Young et al., 2005; Moncuquet et al., 2005). Young et al. (2005) found that, at SOI, the hot electron temperature was a few hundred to a few thousand eV, indicating a longitudinal or temporal variation. They also found the hot electron temperature increased with decreasing radial distance and the fraction of hot electron ranged from 0.01% to 5% within 3–5 R_S. This component of hot electrons was neglected in the average plasma torus model above. In addition, Fleshman et al. (2010) modeled the physical chemistry of the Enceladus torus ($\sim$4 R_S) and found that the hot electrons (energy up to 250 eV) do not exceed 1% of the total population. Therefore, it is reasonable to include a component of hot electrons with energy $\sim$400 eV and density $\sim$5.0 cm^{-3} (the fraction $\sim$1%) into the above model, in which case the hot-electron impact ionization will dominate the photoionization. Including this component, the O_2^+ ion density becomes $\sim$510 cm^{-3} and the W^+ ion density becomes $\sim$130 cm^{-3}. Both are in remarkably good agreement with the averaged CAPS data (O_2^+ $\sim$500 cm^{-3} and W^+ $\sim$150 cm^{-3}). This agreement also appears to confirm that the electron environment in this region was hotter at SOI resulting in the O_2^+ density being dominant.

3.2. Modeling at Saturn equinox

When neutral O_2 and H_2 source rates from ring atmosphere decrease to the order of ten percent of the SOI source rate, the neutral O_2 and H_2 density near the equator drops to roughly one percent of the value at SOI. Therefore, it is surprising that O_2^+ is seen in this region by CAPS as Saturn approaches equinox. However, using the model described above O_2^+ is also formed in this region of the Enceladus torus by ion–molecule reactions. The primary pathway for formation of O_2^+ at equinox is the reaction of OH^+ with O.

Using the intermediate source rate in Table 1, we obtain an average O_2^+ density $\sim$10 cm^{-3} and a total water-group ion density $\sim$20 cm^{-3}. Near equinox, not only does the photolytic O_2 source rate drop, but the solar activity was at a minimum corresponding to reduced photoionization rates for solar minimum (Huebner et al., 1992). Reducing the photolytic source rate, the O_2^+ density becomes $\sim$3 cm^{-3} and the total W^+ density becomes $\sim$15 cm^{-3} in the region of interest near equinox. Results obtained using both an intermediate phase and equinox ring atmosphere are roughly consistent with the average plasma densities observed by CAPS between 2005 and 2010 (Elrod et al., submitted for publication). In addition to the consistency with the temporal variation in the ion densities, our model shows that the main ion species is O_2^+ at SOI while W^+ dominates near equinox, which is also in agreement with the CAPS data. The CAPS data also showed that the average ratio, O_2^+/W^+ decreased from $\sim$2.5–4.5 at SOI to $\sim <1$ near equinox. Although the scatter in the ratios for the later passes is significant this is roughly consistent with our model results.

Because the relative ion–neutral collision speeds are relatively low in this region of the magnetosphere, ion–molecule reactions play an important role on the ion composition favoring for formation of H_3O^+ and O_2^+ as seen above. The low relative speeds lead to relatively large cross-sections but also significant scattering of the ions. Test simulations without ion–molecule collisions were carried out for comparison and are shown in Table 3. It is clearly seen that the ion–molecule reactions significantly alter not only the ion composition but also the total ion densities. Obviously, the predicted seasonal variation of the ring atmosphere (Tseng et al., 2010) has an impact on the seasonal variations of plasma environment observed by CAPS. However, the O_2^+ density is not as sensitive to the variations of neutral O_2 density as one might expect since the reaction of $OH^+ + O$ in the Enceladus torus can produce a small amount of O_2^+. When ion–molecule reactions are included, the total ion densities decrease because the molecular ions, H_3O^+ and O_2^+, are end-products that are more quickly lost to recombination than atomic ions. In fact, the ion–electron recombination rate of H_3O^+ for $T_e \sim 2$ eV is about one order of magnitude higher than other molecular ions accounting for a higher ratio of O_2^+ to W^+ at SOI. Therefore, the results presented here are very sensitive to T_e.

Table 3
Ion densities produced by with/out ion–molecule reactions.

Case	No ion–molecule reactions (cm^{-3})	With ion–molecule collisions (no hot electron with T_e=400 eV) (cm^{-3})
SOI	$W^+ \sim 650$ (mainly O^+) $O_2^+ \sim 10$	$W^+ \sim 20$ (mainly H_3O^+ and H_2O^+) $O_2^+ \sim 150$
Equinox	$W^+ \sim 40$ (mainly O^+) $O_2^+ \sim 0.01$	$W^+ \sim 15$ (mainly H_3O^+ and H_2O^+) $O_2^+ \sim 3$

3.3. O_2^+/W^+ ratio at SOI

As shown above, in absence of the hot electron component with a T_e=400 eV, we calculate total ion densities at SOI that are lower than the CAPS data, especially for the W^+ ions. Although the inclusion of a hot electron component appears to resolve this, we explore other possibilities for the lower model ion densities and the high O_2^+/W^+ ratio at SOI. First, since Smith et al. (2010) found that Enceladus' plumes were likely variable, the contribution of the Enceladus neutral torus could be much higher at SOI not only affecting the O and OH deposited onto the A-ring, but also producing more water-group neutrals in the region of interest. In addition, we ignored the scattered atomic oxygen from dissociation of ring O_2 atmosphere. Third, the interaction of returning hydrogen on the ring particles, affecting the ring H_2 atmosphere enhancement, is uncertain, which in turn can affect the W^+ density through ion–molecule collisions.

To see if the Enceladus' plumes were much more active at SOI, the broad oxygen cloud with a total number of O atoms inside 10 R_S observed by Cassini UVIS before SOI (Esposito et al., 2005; Melin et al., 2009) was used estimate the Enceladus source rate at that time. Assuming that the oxygen atoms are mainly from dissociation of H_2O from the Enceladus' plumes, then $\sim 2.7 \times 10^{34}$ O atoms would be present in steady state if the Enceladus source rate is $\sim 0.85 \times 10^{28}$ s^{-1} (Cassidy, in private communication). This estimate is within about 20% of the ~ 3.1–3.4×10^{34} O atoms reported by UVIS, so that the Enceladus plume source at SOI appears to be reasonably close to what is considered to be the average source rate.

Another possible effect on the water-group ion density is the oxygen atoms scattered out of the ring atmosphere, which were neither included in the Tseng et al's. (2010) calculation nor in the correction for the ring particles temperature calculated here. Based on our model of the ring O_2 atmosphere, the oxygen atoms are mainly produced by photodissociation of O_2 and charge transfer between O^+ and O_2. Due to rapid loss to the ring absorption, which also contributes to the O_2^+ enhancement discussed earlier, the ring component of the atomic oxygen density is $\sim$2000–4000 cm^{-3} near equator at 2.5–3 R_S. Although this is slightly larger than the oxygen population in the Enceladus' water torus ($\sim$1000 cm^{-3} in Cassidy and Johnson (2010)), the additional O increases the W^+ ion density by only $\sim$10% when photoionization dominates.

As mentioned before, the magnetosphere at SOI was very compressed (e.g. Bunce et al., 2005) so that the SOI plasma environment differs from the average environment. Therefore,

including a component of hot electrons with a temperature T_e=400 eV and density N_e=5 cm^{-3} (~1% of the total electron density), resulted in ion densities and an O_2^+/W^+ ratio that were in good agreement with the SOI data as discussed in Section 3.1. The hot electrons affect the ratio by producing more W^+ ions (compared to O_2^+) than photoionization (see reaction rates in Appendix 1). Interestingly, with a hot electron component, the O_2^+/W^+ ratio becomes insensitive to the very uncertain H_2 enhancement factor. Vice versa, for a fixed H_2 density, the total ion density decreases and the O_2^+/W^+ ratio increases when the hot electron component decreases.

4. Plasma temperature

Our analysis of the CAPS data showed that there were not only the drastic variations in the ion densities and composition from 2004 (SOI) to 2010, but also a significant drop in the ion temperature from SOI to the 2005–2010 era (Elrod et al., submitted for publication). At SOI the ion temperatures were close to pickup energy, but were, roughly, less than half that for 2005–2010. Although there were considerable uncertainties in the plasma flow speeds obtained from our 1D fit to the data, which could affect the temperature estimates, the flow speeds were reasonably close to, or slightly larger than, the co-rotational velocity for all the examined passes. Following the pick-up of newly formed ions, the ion temperature can be modified by a number of processes including diffusion and the interactions with the electrons and neutrals. Therefore, to understand the low ion temperatures detected by CAPS, we simultaneously solved the set of continuity equations for density and energy (temperature) for each ion species and the thermal electron. That is, we added the energy equations into the ion-chemistry model in Section 3.

Once ionized by the photons, electrons and charge exchange reactions, an ion newly formed near the equator is picked-up i.e., it is accelerated to the corotation speed, V_{co}, and attains a gyromotion with an energy $E_P=1/2m_iVrel^2$ where $Vrel$ ($=V_{co}-V_{orb}$) with V_{orb} the local Keplerian speed. Since the distribution isotrophizes fairly rapidly by wave particle scattering and mutual collisions, the motion about the mean flow is often characterized by a temperature, kT_i-E_P. Using this as the initial thermal energy, the energy loss processes are considered. One such process is the Coulomb interactions between ions and electrons. The suprathermal electron population (a few hundred to a few thousand eV) in this region is, typically, negligible but a small population of intermediate-hot electrons, the fresh photoelectrons, is usually present (Schippers et al., 2009). However, as mentioned before, a population of hot electron with T_e~100–3000 eV was detected at SOI with a fraction that varied between 0.01% and 5% within 3–5 R_S (e.g., Young et al., 2005). The thermal equilibration rate due to Coulomb interactions between ions and electrons is given by

$$\gamma_\beta^\alpha = 1.8\times10^{-19}\frac{(m_\alpha m_\beta)^{1/2}z_\alpha^2 z_\beta^2 n_\beta \lambda_{\alpha\beta}}{(m_\alpha T_\beta + m_\beta T_\alpha)^{3/2}}$$

where $\lambda_{\alpha\beta}$ ~10–20 is the Coulomb logarithm (Book, 1990). Energy loss from the ion population also occurs by ion–electron recombination, by radial diffusion, and by momentum transfer during ion–molecule collisions. These aspects are all accounted for in the following.

To approximate the momentum transfer in ion–molecule reactions, the reaction rates between ions and neutrals are determined by the Langevin rate constant, $2\pi[\alpha(Ze)^2/m_i]^{0.5}$ where α is the polarizability of neutrals (e.g. Johnson et al., 2006). This rate constant, applicable for slow collisions, is a measure of the size of the region for which the ion and neutral interact strongly and roughly share the center of mass energy. For near-equal mass collisions this implies that about half the ion energy lost to neutrals (see Appendix 2).

The thermal electron energy is determined by cooling to the neutral water molecules, energy loss to radial transport and recombination, and heating by the Coulomb interactions with ions and hot electrons. A new electron formed by photoionization is given an excess energy obtained from Huebner et al. (1992). Due to very large electron-impact cross sections for rotational and vibrational excitation of polar molecules, cooling only by water molecules is taken into account. This is consistent with what occurs in cometary ionospheres (Cravens and Korosmezey, 1986). Although neutral O_2 is dominant at SOI, electron cooling to O_2 is negligible, since the energy loss cross sections are about two orders-of-magnitudes smaller than those for H_2O at T_e~2 eV. The cooling rates with H_2O are assumed to be half the values used in Cravens and Korosmezey (1986) based on a recent review of rotational cross sections (Itikawa, 2007; Cravens et al., 2011).

4.1. Modeling results: thermal electron temperature

We simultaneously solve for plasma densities and energies at both SOI and equinox using the neutral densities discussed in Section 3. The ion densities attained are about the same as the values given in Table 3 in which the ion temperature was ignored. Our modeling of the thermal electron temperature gives ~1–2.5 eV, which is in good agreement with the Cassini observations (e.g. Tokar et al., 2006, 2008). We also note that the thermal equilibration time between heavy ions (e.g. W^+ and O_2^+) and electrons is approximately 10^6–10^7 s, which is much longer than the plasma lifetime, ~a few × 10^5 s, due to recombination. Therefore, Coulomb collision with the heavy ions is not an efficient electron heating mechanism. For heating by the protons the equilibrium time is faster, ~a few × 10^5 s, but the proton density is low (~10% of W^+ density) so the net effect is again small. The heating of thermal electrons by the co-rotating proton population has been discussed in Rymer et al. (2007) and Sittler et al. (2006). On the other hand, we find that the equilibration time between thermal electrons and the hot electrons is ~10^3–10^4 s, which makes this an important heat source, with electron–water cooling the dominant loss process. Gustafsson and Wahlund (2010) and Cravens et al. (2011) had the similar conclusions in their studies of the electron energy in Saturn's inner magnetosphere and in Enceladus' water torus.

4.2. Modeling results: ion temperature

Using the above model which includes the hot electron component, we obtain thermal energies for O_2^+ of ~32 eV at SOI and ~12 eV at equinox as well as W^+ energies of ~20 eV at SOI and ~11 eV at equinox. These average energies are close to ~80%–100% of normal pickup temperature (~20 eV for W^+ ions and ~40 eV for O_2^+ ions at 3.0 R_S) for SOI conditions and ~30%–70% of pickup temperature energy for both intermediate and equinox ring atmosphere conditions. Since cooling to the electrons is inefficient, as discussed above, the low ion temperatures are mostly a result of the energy exchange during ion–molecule collisions. These compare favorably with the CAPS data which indicated that the ions were near pickup energy at SOI but near equinox were ~50% of pickup energy (Elrod et al., submitted for publication).

From this analysis it appears that the momentum transfer during low relative-speed ion–molecule collisions might account for the low ion temperatures detected by CAPS. Johnson et al.

(2006) also calculated the scattered ion energy distribution in the co-rotating frame for very low relative-speed collisions of O_2^+ ions and neutral O_2 molecules over the main rings. The result, shown in their Figure 2, deviated significantly from an isotropic Maxwellian energy distribution so more detailed simulations are needed in future work. For example, the significant ion temperature anisotropy has been ignored but is clearly important requiring a 3D analysis of the CAPS data that is now in progress. In addition, calculating the energy exchange between ions and electrons, we assumed a Maxwellian distribution while the fresh pickup ions have a "pancake (or ring)" distribution (e.g. Tokar et al., 2008). This may in part explain the modeled electron temperature being slightly lower than the detected values as suggested by Gustafsson and Wahlund (2010) and Cravens et al. (2011).

4.3. Interactions with dust

The region of interest, between 2.5 and 3.5 R_S, is permeated with dust particles from the F, G and E rings. The F ring, a narrow structure just outside of the A ring, is dynamic, changing rapidly both spatially and temporally, even on time scales of hours (Murray et al., 2008). One of Saturn's mysterious rings, the G ring, is $\sim$2.8 R_S from the center of the planet, the outer edge or our region. The entire G ring could be derived from an arc of debris held in resonance with Mimas and produced by micro-meteorite impacts generating ejecta that subsequently spreads out (Hedman et al., 2007). The depletions of energetic electrons detected by Cassini MIMI suggested that a lot more small grains are distributed within the ring than is seen by Cassini cameras (Roussos et al., 2005). The diffusive E ring is populated by the icy particles and dust emanating from Enceladus' south pole. All these rings are composed of sub-micron and micron-sized grains (e.g. Hedman et al., 2007; Kempf et al., 2008; Horanyi et al., 2009). The Cassini CDA data showed the dust density of grains larger than 0.8 μm is $\sim 2\times10^{-3}$ m^{-3} near Mimas' orbit and the peak density at $\sim$4.0 R_S is $\sim$0.2 m^{-3} (Kempf et al., 2008). However, the dust density of smaller particles would be much higher since the dust population follows a steep size distribution with r_d^{-a} where r_d is the grain radius ($a\sim$4–5 from Kempf et al., 2008).

In this dusty plasma, the grains are charged a few volts negatively (Jurac et al., 1995; Kempf et al., 2006). Charged grains larger than micron-sized in the E ring have velocities comparable to the local Keplerian velocity (e.g. Hamilton and Burns, 1994). The smaller charged grains have velocities between the local Keplerian velocity and the co-rotational plasma velocity. Because the Debye length is generally around a few meters, which is smaller than the inter-grain distance, the grains act as isolated screened particles. The momentum transfer between the ions and the charged dust occurs at a rate ($\sim\sigma n_d V_{rel}$). σ is the screened Coulomb cross-section, which at these electron densities is $\sim 2\times10^{-6}$ cm^2. With an average dust density (n_d)$\sim 2\times10^{-9}$ cm^{-3} and relative velocity, $V_{rel}\sim 1.5\times10^6$ cm s^{-1} at 3.0 R_S, the ion–dust interaction time is $\sim 2\times10^8$ s. Since this is much longer than the ion lifetime, $\sim$a few times $\times 10^5$ s due to recombination, ions do not even experience one interaction with the dust prior to their loss. Therefore, ion–dust collisions cannot account for the low ion temperatures detected in CAPS data in 2005–2010.

5. Summary

To understand the surprisingly large changes in the ion density, temperature and composition between solstice and equinox revealed by Cassini CAPS (Elrod et al., submitted for publication), we carried out simulations of seasonal variations in Saturn's plasma environment near the equatorial plane between 2.5 and 3.5 R_S. We used a revised ring atmosphere model in which we accounted for the temporal change in the average ring particle temperature as well as the change in the solar incident angle with respect to the ring plane. This resulted in a more drastic seasonal variation than our previous prediction in Tseng et al. (2010) although there are still considerable uncertainties on the importance of oxygen recycling on the surfaces of the ring particles. Combining the water-group neutrals from Enceladus torus and the O_2 and H_2 molecules from the ring atmosphere, our one-box ion-chemistry model can reasonably account for the large variations in the ion densities and composition between SOI and equinox observed by CAPS if we assume the magnetosphere was highly compressed so that a hot component of electrons was present at SOI. It also suggests that the relatively low-speed ion–molecule reactions in this region produce measurable amounts of O_2^+ even with a severely quenched ring atmosphere near equinox. This does not take place in the magnetosphere outside Enceladus because of increasing the relative collision speed. However, there are still other constraints on this model such as interactions with dust grains, neutral sources from radiolytic decomposition of small icy dust in this region, and so on. These will be explored in more detail in future. Also, the modeling described here confirms our conclusion in Elrod et al. (submitted for publication) about predicted seasonal variations in the ring atmosphere. We showed that:

(1) Including the orientation of the ring plane to the Sun and the seasonal variation of ring particle temperature, the neutral O_2 source rate for the ring atmosphere is $\sim 2.0\times10^{27}$ s^{-1} at SOI (solstice) by scaling to CAPS data (Elrod et al., submitted for publication). Near equinox, it is $\sim 2.0\times10^{25}$ O_2 s^{-1} allowing for the same enhancement factor due to recycling.

(2) O_2 and H_2 scattered from the ring atmosphere by ion–molecule collisions are important sources for the magnetosphere (Johnson et al., 2006; Martens et al., 2008; Tseng et al., 2010) as are the water products from Enceladus neutral torus (Cassidy and Johnson, 2010). These sources are included in an ion-chemistry model to describe the temporal changes in ion densities, temperatures and composition detected by CAPS. Our results show that, at SOI, the O_2^+ ion density is $\sim$510 cm^{-3} and the W^+ ion density is $\sim$130 cm^{-3}. We also find that O_2^+ density is $\sim$3 cm^{-3} and a total W^+ density is $\sim$15 cm^{-3} near equinox. Both are in good agreement with the averaged CAPS data. Therefore, in the region between 2.5 and 3.5 R_S, although the possible variability in the Enceladus source might contribute, the observed variations in plasma densities and composition were primarily seasonal as predicted.

(3) The ion–neutral collisions, due to low relative speed in this region, play important roles on the observed composition and the surprisingly low ion temperatures found in the plasma data close to equinox. Based on the dust density in this region (Kempf et al., 2008), the ion–dust interaction appears to be negligible.

(4) Our model indicates that the presence of hot electrons at SOI (T_e=400 eV) plays a dominant role in determining both the ion densities and composition. In the absence of a significant hot electron component photoionization dominates and the H_2 from the ring atmosphere becomes important in determining the W^+ density. In spite of the larger scale height over the ring plane for the H_2 than that for O_2, CAPS should have detected H_2^+ ions in the Cassini division at SOI if H_2 and O_2 are formed in the ring atmosphere with a stoichiometric ratio of 2:1 and the enhancements due to recycling were similar (Tseng et al., 2011). Therefore, the actual H_2 density in our region remains uncertain requiring continued analysis of CAPS data.

In spite of the uncertainties mentioned, it is exciting that the predicted seasonal variations in the ring atmosphere appear to account for the significant differences in Saturn's trapped plasma observed by the CAPS instrument on Cassini and earlier by the plasma instrument on Voyager.

Acknowledgment

We thank Prof. Wing Ip for helpful suggestions on the plasma interactions. We also thank Dr. T.A. Cassidy and Dr. Abi Rymer for useful discussions on Enceladus neutral clouds and Saturnian magnetosphere at SOI. This work is supported by a grant from the NASA's Planetary Atmosphere's Program and a subgrant from the Cassini CAPS instrument team at SwRI via a grant through JPL.

Appendix 1

See Tables A1–A4.

Table A1
Photoionization.

Photoionization	Reaction	Rate constant (s^{-1}) (Huebner et al., 1992) Above: Solar min Below Solar max
	$H_2O+h\nu \rightarrow H_2O^+ + e$	3.55D−9 8.9D−9
	$H_2O+h\nu \rightarrow OH^+ + H + e$	5.95D−10 1.62D−9
	$H_2O+h\nu \rightarrow O^+ + H_2 + e$	6.28D−11 2.37D−10
	$H_2O+h\nu \rightarrow H^+ + OH + e$	1.41D−10 4.37D−10
	$OH+h\nu \rightarrow OH^+ + e$	2.65D−9 7.0D−9
	$O+h\nu \rightarrow O^+ + e$	2.15D−9 5.8D−9
	$H+h\nu \rightarrow H^+ + e$	4.8D−9 1.85D−9
	$O_2+h\nu \rightarrow O_2^+ + e$	4.3D−9 1.27D−8
	$O_2+h\nu \rightarrow O^+ + O + e$	1.3D−9 3.73D−9
	$H_2+h\nu \rightarrow H_2^+ + e$	9.1D−10 1.23D−9
	$H_2+h\nu \rightarrow H^+ + H + e$	4.0D−10 3.0D−10

Table A2
Electron impact ionization.

Electron-impact ionization	Reaction	Rate constant $cm^3\ s^{-1}$ (Ref.) Top: T_e=2.0 eV Middle: T_e=25.0 eV Bottom: 400.0 eV
	$O_2+e \rightarrow O_2^+ + 2e$	8.4D−12 (Itikawa, 2009) 3.1D−8 1.2D−7
	$O_2+e \rightarrow O^+ + O + 2e$	1.2D−13 (Itikawa, 2009) 1.2D−8 6.5D−8
	$H_2O+e \rightarrow H_2O^+ + 2e$	1.4D−11 (Itikawa and Mason, 2005) 3.0D−8 8.8D−8
	$H_2O+e \rightarrow OH^+ + H + 2e$	3.0D−13 (Itikawa and Mason, 2005) 7.9D−9 2.9D−8
	$H_2O+e \rightarrow O^+ + H_2 + 2e$	2.4D−15 (Itikawa and Mason, 2005) 8.5D−10 4.6D−9
	$H_2O+e \rightarrow H^+ + O_2 + 2e$	5.6D−14 (Itikawa and Mason, 2005) 5.0D−9 2.5D−8
	$OH+e \rightarrow OH^+ + H + 2e$	1.4D−11 [a] 3.0D−8 8.8D−8
	$OH+e \rightarrow O^+ + H + 2e$	3.0D−13 [a] 7.9D−9 2.9D−8
	$OH+e \rightarrow H^+ + O + 2e$	5.6D−14 [a] 5D−9 2.5D−8
	$O+e \rightarrow O^+ + 2e$	6.7D−12 (Kim and Desclaux, 2002) 3.0D−8 1.0D−7
	$H+e \rightarrow H^+ + 2e$	1.2D−12 (Shah et al., 1987) 1.5D−8 2.7D−8
	$H_2+e \rightarrow H_2^+ + 2e$	4.7D−12 (Yoon et al., 2008) 2.1D−8 4.5D−8
	$H_2+e \rightarrow H^+ + H + 2e$	1.8D−15 (Yoon et al., 2008) 1.2D−9 3.3D−9

[a] For simplicity, we apply the same electron-impact cross-section data of H_2O molecules to OH molecules.

Appendix 2. Energy change of pickup ions after scattered by neutrals

Here we examine the effective temperature, or width of the speed distribution, of an ion that is scattered by a neutral and then re-accelerated to co-rotation speed with a corresponding change in the gyromotion. If the scattered ion is moving with an assumed isotropically Maxwellian energy distribution, the average energy in each direction is $\langle m\mathbf{v_i}^2/2\rangle = kT_i/2$. Below we define the width of the energy distribution in each direction and then get a temperature.

For an ion–neutral collision (with equal mass): for a fast collision in which the interaction is weak and the deflections small: $A^+(\mathbf{v_i})+A(\mathbf{v_o}) \rightarrow A(\mathbf{v'_i})+A^+(\mathbf{v_o})$. If before the collision, we write $\mathbf{v_i}=\mathbf{v_{co}}$, the ion velocity after picked up is $\mathbf{v'_i}=\mathbf{v_{co}}+\mathbf{u_p}\mathrm{abs}(\mathbf{v_o}-\mathbf{v_{co}})$ with $\mathbf{u_p}$, a randomly oriented unit vector in 2D perpendicular to the local field line assumed to be in the z direction.

For a slow collision, for which the Langevin cross sections applies and the interaction is strong, $A^+(\mathbf{v_i})+A(\mathbf{v_o}) \rightarrow A((\mathbf{v_i}+\mathbf{v_o})/2+\mathbf{u}_1\mathrm{abs}(\mathbf{v_i}-\mathbf{v_o})/2)+A^+((\mathbf{v_i}+\mathbf{v_o})/2-\mathbf{u}_1\mathrm{abs}(\mathbf{v_i}-\mathbf{v_o})/2)$.

Here $\mathbf{u}_1$ is random in 3D due to the assumed isotropic scattering in the center of mass. We can write $\mathbf{u}_1=\sin\theta\cos\varphi\,\mathbf{x}+\sin\theta\sin\varphi\,\mathbf{y}+\cos\theta\,\mathbf{z}$ with $\mathbf{du}_1=(d\cos\theta\,d\varphi)/4\pi$ where θ is the angle with the z-axis and φ is the azimuthal angle about the z-axis. Therefore, for initial $\mathbf{v_i}=\mathbf{v_{co}}$, the ion velocity after scattering and pick-up is $\mathbf{v'_i}=\mathbf{v_{co}}-\mathbf{u_p}\,\mathrm{abs}((\mathbf{v_{co}}-\mathbf{v_o})/2+\mathbf{u_{1p}}\,\mathrm{abs}(\mathbf{v_{co}}-\mathbf{v_o})/2)+\mathbf{u_{1z}}\,\mathrm{abs}(\mathbf{v_{co}}-\mathbf{v_o})/2$.

After the collisions the width of the energy distribution is $\langle(\mathbf{v_i}'-\mathbf{v_{co}})^2\rangle$ where $\langle\ \rangle$ means average over all the random orientations. Again, assuming that before the collision $\mathbf{v_i}=\mathbf{v_{co}}$

Table A3
Charge transfer collisions.

Charge transfer collisions	Reaction	Rate constant $m^3\ s^{-1}$ (Ref.)
	$H_2O+{+}H_2O\rightarrow OH+H_3O^+$	$7.5D-10$ (Lishawa et al., 1990)
	$H_2O+{+}H_2O\rightarrow H_2O+H_2O^+$	$1.5D-9$ (Lishawa et al., 1990)
	$H_2O^+ + OH\rightarrow O+H_3O^+$	$6.9D-10$ (Ip, 1997)
	$H_2O^+ + O\rightarrow H_2+O_2^+$	$4.0D-11$ (Ip, 1997)
	$H_2O^+ + O_2\rightarrow H_2O+O_2^+$	$5.0D-9$ (Fehsenfeld et al., 1967)
	$H_2O^+ + H_2\rightarrow H+H_3O^+$	$8.3D-10$ (Ip, 1997)
	$OH^+ + H_2O\rightarrow OH+H_2O^+$	$1.5D-9$ (Lishawa et al., 1990)
	$OH^+ + H_2O\rightarrow O+H_3O^+$	$1.3D-9$ (Ip, 1997)
	$OH^+ + OH\rightarrow O+H_2O^+$	$7.0D-10$ (Ip, 1997)
	$OH^+ + O\rightarrow H+O_2^+$	$7.1D-10$ (Ip, 1997)
	$OH^+ + O_2\rightarrow OH+O_2^+$	$5.9D-10$ (Ip, 1997)
	$OH^+ + H_2\rightarrow H+H_2O^+$	$1.0D-9$ (Ip, 1997)
	$O^+ + H_2O\rightarrow O+H_2O^+$	$6.1D-9$ (Dressler et al., 2006)
	$O^+ + OH\rightarrow O_2+H^+$	$1.2D-10$ (Giguere and Huebner, 1978)
	$O^+ + OH\rightarrow O+OH^+$	$3.0D-10$ (Giguere and Huebner, 1978)
	$O^+ + O\rightarrow O+O^+$	$1.8D-8$ (Ip, 1997)
	$O^+ + H\rightarrow O+H^+$	$2.0D-9$ (Tawara et al., 1985)
	$O^+ + O_2\rightarrow O+O_2^+$	$2.0D-9$ (Stebbings et al., 1964)
	$O^+ + H_2\rightarrow H+OH^+$	$17D-9$ (Ip, 1997)
	$H^+ + H_2O\rightarrow H+H_2O^+$	$7.4D-10$ (Lindsay et al., 1997)
	$H^+ + OH\rightarrow H+OH^+$	$7.4D-10$ (Lindsay et al., 1997)
	$H^+ + O\rightarrow H+O^+$	$7.0D-10$ (Ip, 1997)
	$H^+ + H\rightarrow H+H^+$	$5.9D-9$ (Tawara et al., 1985)
	$H^+ + O_2\rightarrow H+O_2^+$	$2.1D-9$ (Rees, 1989)
	$H^+ + H_2\rightarrow H+H_2^+$	$3.4D-11$ (Tawara et al., 1985)
	$O_2^+ + O_2\rightarrow O_2+O_2^+$	$7.4D-10$ (Tseng et al., 2010)
	$H_2^+ + H_2O\rightarrow H+H_3O^+$	$3.4D-9$ (Ip, 1997)
	$H_2^+ + H_2O\rightarrow H_2+H_2O^+$	$3.9D-9$ (Ip, 1997)
	$H_2^+ + OH\rightarrow H+H_2O^+$	$7.6D-10$ (Ip, 1997)
	$H_2^+ + OH\rightarrow H_2+OH^+$	$7.6D-10$ (Ip, 1997)
	$H_2^+ + O\rightarrow H+OH^+$	$1.0D-9$ (Ip,1997)
	$H_2^+ + H\rightarrow H_2+H^+$	$6.4D-10$ (Ip,1997)
	$H_2^+ + O_2\rightarrow H_2+O_2^+$	$1.9D-10$ (Tseng et al., 2011)
	$H_2^+ + H_2\rightarrow H_2+H_2^+$	$2.6D-10$ (Tseng et al., 2011)

Table A4
Recombination.

Recombination	Reaction	Rate $m^3\ s^{-1}$ (T_e=2 eV; Schreier et al., 1993)
	$H_3O^+ + e\rightarrow H_2O+H$	$3.5D-8$
	$\rightarrow OH+H_2$	$2.34D-8$
	$\rightarrow OH+H+H$	$6.5D-7$
	$H_2O^+ + e\rightarrow OH+H\rightarrow O+H_2$	$4.5D-8$
	$OH^+ + e\rightarrow O+H$	$8.5D-9$
	$O^+ + e\rightarrow O$	$4.0D-12$
	$O_2^+ + e\rightarrow O+O$	$2.5D-8$
	$H^+ + e\rightarrow H$	$1.3D-13$
	$H_2^+ + e\rightarrow H_2$	$4.0D-8$
Diffusion time		~2 months (~$5.2D6$ s; Rymer et al., 2008)

with co-rotation in the **x** direction for a fast collision with weak interaction (like an ionization), then the integral over the random directions is $\int(\mathbf{v'_i}-\mathbf{v_{co}})^2\mathbf{du_p}=(\mathbf{v_{co}}-\mathbf{v_o})^2$, or the width in each direction (**x** and **y**) is $(v_{co}-v_o)^2/2$ so that $kT_i/2=(m/2)(\mathbf{v_{co}}-\mathbf{v_o})^2/2$ or $kT_i=m(\mathbf{v_{co}}-\mathbf{v_o})^2/2$. On the other hand, for a slow collision with an strong interaction, then

$$\int\int(\mathbf{v'_i}-\mathbf{v_{co}})^2\mathbf{du_1 du_p}=\int\int[\mathbf{u_p}\ \mathrm{abs}((\mathbf{v_{co}}-\mathbf{v_o})/2 + \mathbf{u_{1p}}\ \mathrm{abs}(\mathbf{v_{co}}-\mathbf{v_o})/2)+\mathbf{u_{1z}}\ \mathrm{abs}(\mathbf{v_{co}}-\mathbf{v_o})/2]^2\mathbf{du_1\ du_p}$$
$$=\int\int[(\mathrm{abs}((\mathbf{v_{co}}-\mathbf{v_o})/2+\mathbf{u_{1p}}\ \mathrm{abs}(\mathbf{v_{co}}-\mathbf{v_o})/2))^2 + (\mathrm{abs}(\mathbf{v_{co}}-\mathbf{v_o})/2)^2]\mathbf{du_1\ du_p}$$
$$=((\mathbf{v_{co}}-\mathbf{v_o})/2)^2\int((1+2(\mathbf{u_{1p}})_\mathbf{x}+\mathbf{u_{1p}}^2)+1)\mathbf{du_1\ du_p}$$
$$=(\mathbf{v_{co}}-\mathbf{v_o})^2/2.$$

That is the width is half of that above which is the simple result used in our ion energy analysis.

It would be clearer to break down into **x**, **y**, **z** directions:

$$kT_z/2=(m/2)\int\int[\cos\theta\ \mathrm{abs}(\mathbf{v_{co}}-\mathbf{v_o})/2]^2\mathbf{du_1} = [(\mathbf{v_{co}}-\mathbf{v_o})/2]^2/3=(1/12)(m/2)(\mathbf{v_{co}}-\mathbf{v_o})^2$$
$$kT_x/2=(m/2)((\mathbf{v_{co}}-\mathbf{v_o})/2)^2\int\int\cos\alpha^2[(1+\sin\theta\cos\varphi)^2 + (\sin\theta\sin\varphi)^2]\mathbf{du_1\ du_p}$$
$$=(m/2)((\mathbf{v_{co}}-\mathbf{v_o})/2)^2\int(1/2)[(1+\sin\theta\cos\varphi)^2 + (\sin\theta\sin\varphi)^2]\mathbf{du_1}(5/24)(m/2)(\mathbf{v_{co}}-\mathbf{v_o})^2.$$

Since $kT_x/2=kT_y/2$, then $3kT_i/2=[(5/24)+(5/24)+(2/24)](m/2)(\mathbf{v_{co}}-\mathbf{v_o})^2=(m/2)(\mathbf{v_{co}}-\mathbf{v_o})^2/2$ as above. In Johnson (1990) and Johnson et al. (2006) cases in which the ion initially has gyromotion are considered. The resulting distribution is seen to be much narrower than a Maxwellian.

References

Book, D.L., 1990. NRL Plasma Formulary. Naval Res. Lab., Washington, DC.

Bunce et al., 2005. In situ observations of a solar wind compression-induced hot plasma injection in Saturn's tail, Geophysical Research Letters, 32, 20, http://dx.doi.org/10.1029/2005GL022888.

Cassidy, T.A., Johnson, R.E., 2010. Collisional spreading of Enceladus' neutral cloud. Icarus 554 (209), 696–703, http://dx.doi.org/10.1016/j.icarus.2010.04.010.

Coates, A.J., McAndrews, H.J., Rymer, A.M., Young, D.T., Crary, F.J., Maurice, S., Johnson, R.E., Baragiola, R.A., Tokar, R.L., Sittler, E.C., Lewis, G.R., 2005. Plasma electrons above Saturn's main rings: CAPS observations. Geophysical Research Letters 32, 14, http://dx.doi.org/10.1029/2005GL022694.

Cravens, T.E., Korosmezey, A., 1986. Vibrational and rotational cooling of electrons by water vapor. Planetary and Space Science 34, 961–970, http://dx.doi.org/10.1016/0032-0633(86)90005-X.

Cravens, T.E., Ozak, N., Richard, M.S., Campbell, M.E., Robertson, I.P., Perry, M., Rymer, A.M., 2011. Electron energetics in the Enceladus torus. Journal of Geophysical Research 116, 9, http://dx.doi.org/10.1029/2011JA016498.

Dressler, R.A., Bastian, M.J., Levandier, D.J., Murad, E., 2006. Emperical model of the state-state dynamics in near-resonant hyperthermal $X^+ + H_2O$ charge-transfer reactions. International Journal of Mass Spectrometry 159, 245–256.

Elrod, M.K., Tseng, W.-L., Wilson, R.J., Johnson, R.E., 2012. Seasonalvariations in Saturn's plasma between the main rings and Enceladus'. Journal of Geophysical Research 117, A3, CiteID A03207, http://dx.doi.org/10.1029/2011JA017332.

Esposito et al., 2005, Ultraviolet Imaging Spectroscopy shows an Active Saturnian system, Science, 307, 5713 pp. 1251–1255 , http://dx.doi.org/10.1126/science.1105606.

Farrell, W.M., Kaiser, M.L., Gurnett, D.A., Kurth, W.S., Persoon, A.M., Wahlund, J.E., Canu, P., 2008. Mass unloading along the inner edge of the Enceladus plasma torus. Geophysical Research Letters 35, L02203.

Fehsenfeld, F.C., Schmeltekopf, A.L., Ferguson, E.E., 1967. Thermal energy ion-neutral reaction rates, VII, Some hydrogen-atom abstraction reactions. Journal of Chemical Physics 46, 2802.

Flandes, Alberto, Spilker, Linda, Morishima, Ryuji, Pilorz, Stuart, Leyrat, Cédric, Altobelli, Nicolas, Brooks, Shawn, Edgington, Scott G., 2010. Brightness of Saturn's rings with decreasing solar elevation. Planetary and Space Science 58, 1758–1765, http://dx.doi.org/10.1016/j.pss.2010.04.002.

Fleshman et al., 2010, A sensitivity study of the Enceladus torus, Journal of Geophysical Research, 115, E04007, http://dx.doi.org/10.1029/2009JE003372.

Giguere, P.T., Huebner, W.F., 1978. A model of comet comae, I, gas phase chemistry in one dimension. Astrophysical Journal 223, 638.
Gustafsson, G., Wahlund, J.-E., 2010. Electron temperatures in Saturn's plasma disc. Planetary and Space Science 58, 1018, http://dx.doi.org/10.1016/j.pss.2010.03.007.
Hamilton and Burns, 1994, Origin of Saturn's E Ring: Self-Sustained, Naturally. Science 264, 5158, pp. 550-553, http://dx.doi.org/10.1126/science.264.5158.550.
Hansen, C.J., Shemansky, D.E., Esposito, L.W., Stewart, A.I.F., Lewis, B.R., Colwell, J.E., Hendrix, A.R., West, R.A., Waite Jr, J.H., Teolis, B., Magee, B.A., 2011. The composition and structure of the Enceladus plume. Geophysical Research Letters 38, 11202, http://dx.doi.org/10.1029/2011GL047415.
Horanyi et al., 2009, Saturn from Cassini-Huygens: Diffuse Rings, by Dougherty, Esposito, Krimigis, ISBN 978-1-4020-9216-9. Springer p. 511, http://dx.doi.org/10.1007/978-1-4020-9217-6_16.
Huebner, W.F., Keady, J.J., Lyon, S.P., 1992. Solar photo rates for planetary atmospheres and atmospheric pollutants. Astrophysics and Space Science 195, 1–295.
Ip, W.-H., 1997. On the neutral cloud distribution in the Saturnian magnetosphere. Icarus 126, 42–57, http://dx.doi.org/10.1006/icar.1996.5618.
Itikawa, Y., 2007. Electron collisions with molecules, in molecular processes in plasmas: collisions of charged particles with molecules. Atomic, Molecular, Optical and Plasma Physics, 43. Springer, Berlin, pp. 57–125.
Itikawa, Y., 2009. Cross sections for electron collisions with oxygen molecules. Journal of Physical and Chemical Reference Data 38 (1), 1–20.
Itikawa, Y., Mason, N., 2005. Cross sections for electron collisions with water molecules. Journal of Physical and Chemical Reference Data 34 (1), 1–22.
Johnson, R.E., 1990. Electronically-induced sputtering (desorption), Ion Formation from Organic Solids, pp. 189–195.
Johnson, R.E., Luhmann, J.G., Tokar, R.L., Bouhram, M., Berthelier, J.J., Siler, E.C., Cooper, J.F., Hill, T.W., Smith, H.T., Michael, M., Liu, M., Crary, F.J., Young, D.T., 2006. Production, ionization and redistribution of O_2 Saturn's ring atmosphere. Icarus 180, 393–402, http://dx.doi.org/10.1016/j.icarus.2005.08.021.
Johnson, R.E., 2011. Photolysis and radiolysis of water ice. In: Khriachtchev, L. (Ed.), Physics and Chemistry at Low Temperatures. Pan Stanford Publishing Pte. Ltd., World Scientific, Singapore, pp. 297–339. (Chapter 10).
Jurac, S., Johnson, R.E., Baragiola, R.A., Sittler, E.C., 1995. Charging of ice grains by low-energy plasma: Aplication to Saturn's E ring. Journal of Geophysical Research 100, 14,821–14,831.
Jurac, S., Richardson, J.D., 2007. Neutral cloud interaction with Saturn's main rings. Geophysical Research Letters 34, L08102.
Kempf et al., 2006, The electrostatic potential of E ring particles, Planetary and Space Science, 54, 9-10, p. 999-1006, http://dx.doi.org/10.1016/j.pss.2006.05.012.
Kempf et al., 2008, The E ring in the vicinity of Enceladus. I. Spatial distribution and properties of the ring particles, Icarus, 193, 2, p. 420-437, http://dx.doi.org/10.1016/j.icarus.2007.06.027.
Kim, Y.-K., Desclaux, J.P., 2002. Ionization of carbon, nitrogen, and oxygen by electron impact. Physical Review A 66, 012708.
Krimigis, S.M., et al., 2005. Dynamics of Saturn's magnetosphere from MIMI during Cassini's orbital insertion. Science 307, 1270–1273.
Lindsay, B.G., Sieglaff, D.R., Smith, K.A., Stebbings, R.F., 1997. Charge transfer of 0.5-, 1.5-, and 5-keV protons with H_2O: absolute differential and integral cross sections. Physical Review A 55, 3945–3946.
Lishawa, C.R., et al., 1990. Journal of Chemical Physics 93, 3196–3206.
Martens, H.R., Reisenfeld, D.B., Williams, J.D., Johnson, R.E., Smith, H.T., 2008. Observations of molecular oxygen ions in Saturn's inner magnetosphere. Geophysical Research Letters 35, L20103, http://dx.doi.org/10.1029/2008GL035433.
Melin et al., 2009, The distribution of atomic hydrogen and oxygen in the magnetosphere of Saturn, Planetary and Space Science, Volume 57, Issue 14-15, p. 1743-1753, ''http://dx.doi.org/10.1016/j.pss.2009.04.014"10.1016/j.pss.2009.04.014.
Moncuquet et al., 2005, Quasi thermal noise spectroscopy in the inner magnetosphere of Saturn with Cassini/RPWS: Electron temperatures and density, Geophysical Research Letters, 32, L20S02 http://dx.doi.org/10.1029/2005GL022508.
Murray et al., 2008, Nature 453, 739-744, The determination of the structure of Saturn's F ring by the moonlet http://dx.doi.org/10.1038/nature06999.
Rees, 1989. Physics and Chemistry of the Upper Atmosphere. Cambridge University Press, Cambridge, UK, ISBN: 0521368480, p. 304.
Rossos et al., 2005. Electron microsignatures from the Saturnian satellites: Cassini MIMI/LEMMS observations, American Geophysical Union, Fall Meeting 2005.
Rymer, A.M., et al., 2007. Electron sources in Saturn's magnetosphere. Journal of Geophysical Research 112, A02201, http://dx.doi.org/10.1029/2006JA012017.
Rymer, A.M., Mauk, B.H., Hill, T.W., Paranicas, C., Mitchell, D.G., Coates, A.J., Young, D.T., 2008. Electron circulation in Saturn's magnetosphere. Journal of Geophysical Research 113 (610), A01201, http://dx.doi.org/10.1029/2007JA012589.
Schreier, Ron, Eviatar, Aharon, Vasyliunas, Vytenis M., Richardson, John D., 1993. Modeling the Europa plasma torus. Journal of Geophysical Research 98 (21), 231, http://dx.doi.org/10.1029/93JA02585.
Schippers, P., et al., 2008. Multi-instrument analysis of electron populations in Saturn's magnetosphere. Journal of Geophysical Research, Space Physics 113, A07208.
Schippers, P., André, N., Johnson, R.E., Blanc, M., Dandouras, I., Coates, A.J., Krimigis, S.M., Young, D.T., 2009. Identification of photoelectron energy peaks in Saturn's inner neutral torus. Journal of Geophysical Research, Space Physics 114, A12212, http://dx.doi.org/10.1029/2009JA014368.
Shah, et al., 1987. Pulsed crossed-beam study of the ionisation of atomic hydrogen by electron impact. Journal of Physics B: Atomic and Molecular Physics 20, 3501, http://dx.doi.org/10.1088/0022-3700/20/14/022.
Sittler, E.C., et al., 2006. Cassini observations of Saturn's inner plasmasphere: Saturn orbit insertion results. Planetary and Space Science 54, 1197, http://dx.doi.org/10.1016/j.pss.2006.05.038.
Sittler, E.C., Andre, N., Blanc, M., Burger, M., Johnson, R.E., Coates, A., Rymer, A., Reisenfeld, D., Thomsen, M.F., Persoon, A., Dougherty, M., Smith, H.T., Baragiola, R.A., Hartle, R.E., Chornay, D., Shappirio, M.D., Simpson, D., McComas, D.J., Young, D.T., 2008. Ion and neutral sources and sinks within Saturn's inner magnetosphere: Cassini results. Planetary and Space Science 56, 3–18, http://dx.doi.org/10.1016/j.pss.2007.06.006.
Smith, H.T., Johnson, R.E., Perry, M.E., Mitchell, D.G., McNutt, R.L., Young, D.T., 2010. Enceladus plume variability and the neutral gas densities Saturn's magnetosphere. Journal of Geophysical Research 115, A10252, http://dx.doi.org/10.1029/2009JA015184.
Stebbings, R.F., Smith, A.C.H., Ehrhardt, H., 1964. Charge transfer between oxygen atoms and O+ and H+ ions. Journal of Geophysical Research 69, 2349.
Tawara, H., Kato, T., Nakai, Y., 1985. Cross sections for electron capture and loss by positive ions in collisions with atomic and molecular hydrogen. Atomic Data and Nuclear Data Tables 32, 235, http://dx.doi.org/10.1016/0092640X(85)90007-5.
Thomsen, M.F., Reisenfeld, D.B., Delapp, D.M., Tokar, R.L., Young, D.T., Crary, F.J., Sittler, E.C., McGraw, M.A., Williams, J.D., 2010. Survey of ion plasma parameters in Saturn's magnetosphere. Journal of Geophysical Research 115, A10220, http://dx.doi.org/10.1029/2010JA015267.
Tokar, R.L., et al., 2005. Cassini observations of the thermal plasma in the vicinity of Saturn's main rings and the Fand G rings. Geophysical Research Letters, 32.
Tokar, R.L., et al., 2006. The interaction of the atmosphere of Enceladus with Saturn's plasma. Science 311, 1409, http://dx.doi.org/10.1126/science.1121061.
Tokar, R.L., et al., 2008. Cassini detection of water group pickup ions in the Enceladus torus. Geophysical Research Letters 35, L14202, http://dx.doi.org/10.1029/2008GL034749.
Tseng, W.-L., Ip, W.-H., Johnson, R.E., Cassidy, T.A., Elrod, M.K., 2010. The Structure and time variability of the ring atmosphere and ionosphere. Icarus 206, 382–389, http://dx.doi.org/10.1016/j.icarus.2009.05.019.
Tseng, W.-L., Ip, W.-H., 2011. An assessment and test of Enceladus as an important source of Saturn's ring atmosphere and ionosphere. Icarus 212, 294–299, http://dx.doi.org/10.1016/j.icarus.2010.12.003.
Tseng, W.-L., Johnson, R.E., Thomasen, M.F., Cassidy, T.A., Elrod, M.K., 2011. Neutral H_2 and H_2+ ions in the Saturnian magnetosphere. Journal of Geophysical Research 116, A03209, http://dx.doi.org/10.1029/2010JA016145.
Waite, J.H., Cravens, T.E., Ip, W.-H., Kasprzak, W.T., Luhmann, J.G., McNutt, R.L., Niemann, H.B., Yelle, R.V., Mueller-Wodarg, I., Ledvina, S.A., Scherer, S., 2005. Oxygen ions observed near Saturn's A ring. Science 307, 1260–1262, http://dx.doi.org/10.1126/science.1105734.
Yoon, J.S., Song, M.Y., Han, J.M., Hwang, S.H., Chang, W.S., Lee, B., Itikawa, Y., 2008. Cross sections for electron collisions with hydrogen molecules. Journal of Physical and Chemical Reference Data 37 (2), 913–931.
Young, D.T., Berthelier, J.-J., Blanc, M., et al., 2005. Composition and dynamics of plasma in Saturn's magnetosphere. Science 307, 1262–1266, http://dx.doi.org/10.1126/science.1106151.